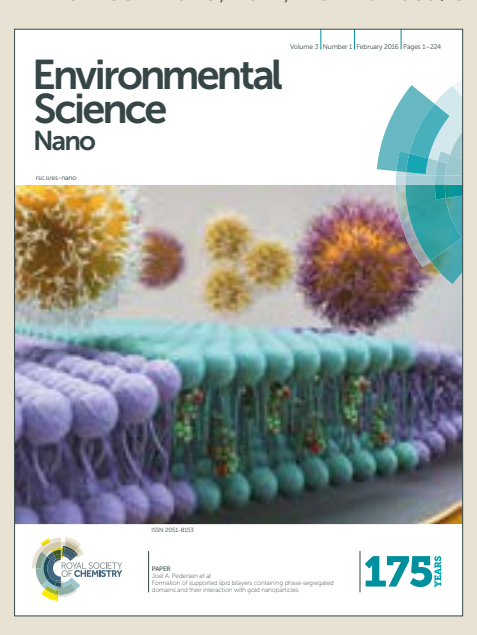
# Check for updates

# **Environmental** Science Nano

Accepted Manuscript





This is an Accepted Manuscript, which has been through the Royal Society of Chemistry peer review process and has been accepted for publication.

Accepted Manuscripts are published online shortly after acceptance, before technical editing, formatting and proof reading. Using this free service, authors can make their results available to the community, in citable form, before we publish the edited article. We will replace this Accepted Manuscript with the edited and formatted Advance Article as soon as it is available.

You can find more information about Accepted Manuscripts in the author guidelines.

Please note that technical editing may introduce minor changes to the text and/or graphics, which may alter content. The journal's standard Terms & Conditions and the ethical guidelines, outlined in our author and reviewer resource centre, still apply. In no event shall the Royal Society of Chemistry be held responsible for any errors or omissions in this Accepted Manuscript or any consequences arising from the use of any information it contains.



Efforts to understand the environmental impact of released nanoparticles have identified some simple relationships between nanoparticle binding and toxicity to bacteria. Here, we use a panel of Gramnegative bacteria that come from diverse environmental niches to assess nanoparticle toxicity and to further understand the interaction of nanoparticles with diverse bacterial cell walls. In using such a panel, we see only a loose correlation between nanoparticle binding amounts and observed toxicity. This demonstrates that more complex biological mechanisms may be involved in nanoparticle toxicity. Using a panel comprised of environmentally-diverse bacteria can help account for biological complexity and allow identification of bacteria types that are most affected by different nanoparticles, which should improve efficiency in investigating the environmental impacts of nanoparticles.



# **Environmental Science: Nano**

# COMMUNICATION

6 Using an environmentally-relevant panel of Gram-negative bacteria to assess the toxicity of polyallylamine hydrochloride-**\*wrapped gold nanoparticles** 

1 Received 00th January 20xx, 2 Accepted 00th January 20xx

3 DOI: 10.1039/x0xx000000x

4 www.rsc.org/

2

4 5

8 9 10

11 12

75155151

Madisonon 1

<u>-</u>28

**⊉**9

iskedon 20

च्<u>च</u>ी वै1

43

44

45

46

47

48

49

50 51

52

53

54

55

56

57

58

59

60

<sup>9</sup> Joseph T. Buchman, <sup>a</sup> Ali Rahnamoun, <sup>b</sup> Kaitlin M. Landy, <sup>a</sup> Xi Zhang, <sup>c</sup> Ariane M. Vartanian, <sup>c</sup> Lisa M. 10 Jacob, <sup>c</sup> Catherine J. Murphy, <sup>c</sup> Rigoberto Hernandez, <sup>b</sup> and Christy L. Haynes<sup>a</sup>

11 We aim to establish the effect of environmental diversity in 38 potential environmental impacts. 1,2 One can probe the potential 21 Binding results showed a general trend that bacteria with smooth 22 LPS bind more PAH AuNPs than bacteria with rough LPS. 23 Computational models reveal that PAH migrates to phosphate 24 groups in the core of the LPS structure. Overall, our results 25 demonstrate that simple interactions between nanoparticles and 26 the bacterial cell wall cannot fully account for observed trends in 27 toxicity, which points to the importance of establishing more modeling 28 comprehensive approaches for 29 nanotoxicity.

#### 30 Introduction

32 high surface-area-to-volume ratio, nanomaterials are increasingly 60 facilitating the binding of nanoparticles with the surface of the model 33 used in consumer products. It is inevitable that, at some stage of the 61 bacterium, S. oneidensis MR-1.16 There are two broad classes of LPS, 34 manufacturing, use, and disposal of such products, some of the 62 designated as either rough or smooth. Rough LPS have a lipid A 35 nanomaterials they contain may be released into the environment. 63 region that anchors the LPS into the membrane and an 36 Therefore, there is a growing focus to understand the behavior of 64 oligosaccharide portion that is bound to the lipid A. By contrast,

12 evaluating nanotoxicity to bacteria. We assessed the toxicity of 4 39 environmental impact through the use of bacterial models, which, as 13 nm polyallylamine hydrochloride-wrapped gold nanoparticles to a 40 decomposers, occupy an important trophic level; decomposers 14 panel of bacteria from diverse environmental niches. The bacteria 41 recycle nutrients that can be used by primary producers. Therefore, 15 experienced a range of toxicities as evidenced by the different 42 any effects on bacteria may impact organisms in other trophic levels, 16 minimum bactericidal concentrations determined; the sensitivities 43 making bacteria a good diagnostic for overall environmental health. 17 of the bacteria was A. vinelandii = P. aeruginosa > S. oneidensis MR- 44 Often, only one bacterial model is used in nanoparticle toxicity 18 4 > A. baylyi > S. oneidensis MR-1. Interactions between gold 45 studies, 4-6 but this can lead to results that may not be generalizable 19 nanoparticles and molecular components of the cell wall were 46 across bacteria from different environments. Therefore, we have 20 investigated by TEM, flow cytometry, and computational modeling.
47 assembled a panel of Gram-negative bacteria with sequenced 48 genomes that occupy different environmental niches for use in 49 nanotoxicity studies.

When evaluating nanoparticle toxicity to bacteria, direct 51 interactions of nanoparticles to the bacterial surface play a role in 52 the toxicity, with several studies demonstrating a correlation 53 between amount of NPs bound to bacteria and observed toxicities. 7environmental 54 10 It has been shown that bound NPs can rupture the bacterial cell 55 membrane, 11,12 lead to alterations in the membrane potential, 13 56 release ions that are localized right at the bacterial surface, 14 and 57 generate reactive oxygen species at the cell membrane. 15 In previous 58 work, we have shown that a main component of the Gram-negative 31 Due to the unique physicochemical properties that arise from their 59 bacterial surface, lipopolysaccharides (LPS), are important in 37 engineered nanomaterials in the environment and determine their 65 smooth LPS have both lipid A and core oligosaccharide regions, with 66 the addition of an O-antigen, a polysaccharide domain bound to the 67 core oligosaccharide, elongating the overall LPS structure. Based on 68 the clear role of LPS in binding nanoparticles, it makes sense to 69 generate a panel that focuses on variation in LPS structure. Such a 70 panel would exclude Gram-positive bacteria, which are also 71 important environmental organisms, but allows us to focus on 72 specific surface chemistry differences between the bacteria used.

Electronic Supplementary Information (ESI) available: Known LPS structures from the bacterial panel, citrate-capped AuNP synthesis, quantification of free PAH, TEM of PAH AuNP binding to bacteria, flow cytometry gating method and supplemental data, and simulation of distance between LPS phosphorus and PAH center of mass. See DOI: 10.1039/x0xx00000x

<sup>&</sup>lt;sup>a.</sup> Department of Chemistry, University of Minnesota, Minneapolis, MN 55455, USA

<sup>&</sup>lt;sup>b.</sup> Department of Chemistry, Johns Hopkins University, Baltimore, MD 21218, USA

<sup>&</sup>lt;sup>c.</sup> Department of Chemistry, University of Illinois at Urbana-Champaign, Urbana, IL

4

75:15:51:21 75:15:51:21 5:15:51 5:15:5

105/27/12 no no sipo-Madison Off States of 105/27/12 no no sipo-madison of the sipo-ma

<u>-</u>28

**⊉**9

December 2017 Downhoaded

43

44

45 46

47

48

49

COMMUNICATION Journal Name

/iew Article Online

Table 1. The bacteria in the panel come from a range of habitats and have different respiration abilities. The panel includes bacteria with cityler/roughson2E smooth LPS presented on their surface. Each bacterium in the panel has an important role in the environment.

<b>Bacterial Strain</b>	Habitat	Respiration	LPS type	<b>Environmental Role</b>
Azotobacter vinelandii UW	Soil <sup>48</sup>	Obligate aerobe <sup>48</sup>	Smooth <sup>49</sup>	Nitrogen cycle
Acinetobacter baylyi ADP1	Soil, sediment, aquatic <sup>18</sup>	Obligate aerobe <sup>18</sup>	Smooth <sup>18</sup>	Metabolize aromatic compounds
Shewanella oneidensis MR-1	Soil, marine <sup>20</sup>	Facultative anaerobe <sup>20</sup>	Rough <sup>25</sup>	Geochemical nutrient cycle
Shewanella oneidensis MR-4	Soil, marine <sup>20</sup>	Facultative anaerobe <sup>20</sup>	Rough <sup>21</sup>	Geochemical nutrient cycle
Pseudomonas aeruginosa PAO1	Ubiquitous <sup>50</sup>	Obligate aerobe <sup>50</sup>	Smooth <sup>51</sup>	Metabolic diversity

The five bacteria that make up the bacterial panel introduced in 31 surface is that the differences in LPS length and composition may 2 this manuscript include *Azotobacter vinelandii* UW, *Acinetobacter* 32 impact their interaction with the NPs used in this study. The 3 baylyi ADP1, Shewanella oneidensis MR-1, Shewanella oneidensis 33 saccharide portions of the LPS structures of *P. aeruginosa*, 23,24 *S.* 4 MR-4, and *Pseudomonas aeruginosa* PAO1. They are a mix of Gram- 34 oneidensis MR-1,25 and *S. oneidensis* MR-4<sup>21</sup> have been elucidated 5 negative bacteria that have smooth or rough LPS on their surface. 35 (Fig. S1), but the LPS structures of the other bacteria in the panel are 6 Differences between the bacteria in the panel are highlighted in 36 not as well characterized. The charges of these LPS structures as well 7 Table 1. In the environment, *A. vinelandii* has an important role in 37 as other LPS structures used in simulations in this manuscript are 8 the nitrogen cycle since it is capable of fixing nitrogen even in the 38 given (Table 2).

9 presence of atmospheric oxygen. <sup>17</sup> The smooth LPS of *A. baylyi* likely <sup>39</sup> To demonstrate the use of the bacterial panel in this manuscript, 10 has branched O-antigens since that is characteristic of the genus 40 each species is exposed to 4-nm-diameter polyallylamine 11 Acinetobacter;18 this bacterium is capable of great metabolic 41 hydrochloride (PAH)-coated gold nanoparticles (AuNPs). AuNPs were 12 diversity, notably in its ability to metabolize aromatic compounds 42 used in this study due to their chemical inertness, size/shape 13 that are often products of plant degradation. 19 S. oneidensis MR-1 43 tunability, and ease of characterization. 26,27 Polyelectrolyte coating is 14 has an important environmental role in geochemical nutrient cycling 44 an industrially-relevant modification of materials as these 15 since it is capable of reducing a wide variety of metals. 20 Similarly, S. 45 functionalized materials have many applications in diverse fields, 28-16 oneidensis MR-4 is also capable of dissimilatory reduction of many 46 30 and this particular coating is known to interact with bacterial 17 different metals.<sup>21</sup> Finally, *P. aeruginosa* PAO1 is an obligate aerobe 47 surfaces and cause membrane disruption as its toxicity 18 that can adapt to live in many different environments due to its 48 mechanism. 7,31 While there is limited work studying PAH AuNPs with 19 metabolic diversity. P. aeruginosa is often used as a biofilm 49 the bacteria in this panel, 32 in previous work, the toxicity of PAH 20 formation model; biofilms may serve as a sink for NPs entering the 50 AuNPs was investigated for S. oneidensis MR-1 using a colony 21 environment, making it likely that P. aeruginosa would encounter 51 counting method. In this manuscript, the effects of the PAH AuNPs 22 nanomaterials that are released into the environment.<sup>22</sup> 52 to each bacterium are noted by determining the minimum

Since these bacteria occupy diverse environmental niches and 53 bactericidal concentration (MBC). The MBC is defined as the lowest 24 have different surface compositions, we expect that they will be 54 nanoparticle concentration that kills at least 99% of the bacteria. This 25 representative of bacteria in the environments that nanoparticles 55 is a facile method to demonstrate the different responses that each 26 may end up in. These differences should also make them suitable for 56 bacterium has to NP exposure. To test the hypothesis that extent of 27 showing a range of responses to nanoparticle exposure so that a 57 NP binding to the bacterial cell surface correlates with toxicity, 28 particular nanoparticle is not deemed non-toxic because a single 58 transmission electron microscopy (TEM) is used to visualize and flow 29 bacterial species happens to be tolerant to it. The motivation for 59 cytometry is used to quantify PAH AuNP binding to each species. In 30 noting the different LPS structures on each bacterial species' cell 60 parallel, a molecular dynamics simulation was used to calculate

Table 2. The number of phosphates and charge of the LPS core polysaccharide structure are provided for several bacterial strain variants (first three rows) and model structures (remaining four rows). O-antigens were entirely absent in all rough model structures and only two O-antigens are included in the "smoother" structure. The PAH used in the simulations has a charge of +10 leading to the total charges listed in the final column. Negative and positive charges were neutralized in the simulations using the corresponding number of sodium cations or chloride anions, respectively.

Bacterial Strain	Number of Phosphate Units	Charge of LPS	Charge of LPS + PAH
S. oneidensis MR-1	5	-7	+3
S. oneidensis MR-4 variant 1	4	-6	+4
S. oneidensis MR-4 variant 2	6	-5	+5
Rough P. aeruginosa PAO1 variant	6	-12	-2
"Smoother" P. aeruginosa PAO1 variant	6	-14	-4
Rough S. typhimurium	4	-10	0
Rough <i>E. coli</i>	5	-9	+1

COMMUNICATION **Journal Name** 

1 relative association energies of the PAH that caps the nanoparticles 51 AuNP characterization 2 for different LPS structures to determine if the presentation of 52 PAH AuNPs were characterized post-synthesis by unit with the presentation of 52 PAH AuNPs were characterized post-synthesis by unit with the presentation of 52 PAH AuNPs were characterized post-synthesis by unit with the presentation of 52 PAH AuNPs were characterized post-synthesis by unit with the presentation of 52 PAH AuNPs were characterized post-synthesis by unit with the presentation of 52 PAH AuNPs were characterized post-synthesis by unit with the presentation of 52 PAH AuNPs were characterized post-synthesis by unit with the presentation of 52 PAH AuNPs were characterized post-synthesis by unit with the presentation of 52 PAH AuNPs were characterized post-synthesis by unit with the presentation of 52 PAH AuNPs were characterized post-synthesis by unit with the presentation of 52 PAH AuNPs were characterized post-synthesis by unit with the presentation of 52 PAH AuNPs were characterized post-synthesis by unit with the presentation of 52 PAH AuNPs were characterized post-synthesis by unit with the presentation of 52 PAH AuNPs were characterized post-synthesis by unit with the presentation of 52 PAH AuNPs were characterized post-synthesis by unit with the presentation of 52 PAH AuNPs were characterized post-synthesis by unit with the presentation of 52 PAH AuNPs were characterized post-synthesis by unit with the presentation of 52 PAH AuNPs were characterized post-synthesis by unit with the presentation of 52 PAH AuNPs were characterized post-synthesis by unit with the presentation of 52 PAH AuNPs were characterized post-synthesis by unit with the presentation of 52 PAH AuNPs were characterized post-synthesis by unit with the presentation of 52 PAH AuNPs were characterized post-synthesis by unit with the presentation of 52 PAH AuNPs were characterized post-synthesis by unit with the presentation of 52 PAH AuNPs were characterized post-synthesis by unit with the presentation of 52 PAH AuNPs with the presentation of 52 PAH AuNPs with the 13 nanomaterials.

#### 14 Materials and Methods

#### 15 Materials

1 2

3

4

5

6 7

8

9

10

11

12

<u>با</u>3

1934 175 175

₹6 27

<u>-</u>28

**⊉**9

December 2017 Downloaded

₹8

299 1390 1390

₹1

42

43

44

45

46

47

48

49 50

51

52

53

54

55

56 57

58

59

60

17 (Na<sub>2</sub>MoO<sub>4</sub>·2H<sub>2</sub>O), 18 acid (HEPES), gold (III) chloride trihydrate (HAuCl<sub>4</sub>·3H<sub>2</sub>O), sodium 19 citrate tribasic dihydrate (C<sub>6</sub>H₅Na₃O<sub>7</sub>·2H₂O), polyallylamine <sup>70</sup> with Burk's medium adapted from Newton, et al<sup>34</sup> were used and 20 hydrochloride (PAH, MW 17.5 kDa), sodium borohydride (NaBH<sub>4</sub>), 21 and sodium chloride (NaCl) were purchased from Sigma-Aldrich 22 (Milwaukee, WI). Potassium phosphate dibasic trihydrate 23 (K<sub>2</sub>HPO<sub>4</sub>·3H<sub>2</sub>O) was purchased from Mallinckrodt (Phillipsburg, NJ). 24 Potassium phosphate monobasic (KH<sub>2</sub>PO<sub>4</sub>) was obtained from J.T. 25 Baker (Center Valley, PA). Dulbecco's phosphate-buffered saline was 26 purchased from Corning (Aurora, CO), LB broth and agar were 27 obtained from BD Difco (Franklin Lakes, NJ). SYTO9 nucleic acid stain 28 was obtained from Molecular Probes (Waltham, MA). Calcium 29 chloride (CaCl<sub>2</sub>) and ferrous sulfate (FeSO<sub>4</sub>) were purchased from 30 Fisher Scientific (Rockford, IL). Absolute anhydrous 99.5% ethanol 31 was obtained from Pharmco-Aaper (Brookfield, CT). All chemicals  $_{32}$  were used as received. Deionized water (18.2 M $\Omega$ ) was purified using  $_{83}$  from the wrapping process. The concentrations of free PAH present 33 a Milli-Q Millipore water purification system (Billerica, MA).

Shewanella oneidensis MR-1 was obtained from Jeffrey Gralnick 35 (Dept of Microbiology, University of Minnesota). Shewanella 36 oneidensis MR-4 was obtained from Daad Saffarini (Dept of Biological 37 Sciences, University of Wisconsin - Milwaukee). Acinetobacter baylyi 38 (ATCC® 33305™), Azotobacter vinelandii (ATCC® 13705™), and 39 *Pseudomonas aeruginosa* (ATCC® 47085™) were purchased from the 40 American Type Culture Collection (Manassas, VA).

#### 41 PAH-coated AuNPs (PAH AuNPs)

42 PAH AuNPs were synthesized by polyelectrolyte wrapping of as-43 synthesized citrate-capped AuNPs (see ESI for synthesis of citrate-44 capped AuNPs).33 To the approximately 3.2 L of as-synthesized 45 citrate-capped AuNPs, 32.0 mL of 100 mM NaCl and 100.0 mL of a 46 PAH solution (MW 17.5 kDa) (10 mg/mL in 1 mM NaCl) was added 47 with vigorous stirring. The solution was stirred overnight and 48 concentrated to around 30 mL by diafiltration cassettes (Tangential 50 AuNPs were purified by centrifugation at 13,000×q for 55 min.

3 negatively charged phosphate groups facilitates the interaction of 53 spectroscopy, TEM, and ζ-potential measurement. The size and ζ-4 LPS with the amine groups of PAH. Taken together, the results 54 potential for the PAH AuNPs were also characterized in the exposure 5 demonstrate that a simple hypothesis related to the molecular 55 medium using UV-vis extinction spectroscopy and ζ-potential 6 character of the LPS is not sufficient to explain the nanoparticle 56 measurement. UV-vis extinction spectra post-synthesis were 7 association and toxicity results. This is a benefit to using such a panel, 57 obtained on a Cary 500 UV-vis-NIR spectrophotometer and the 8 as it identifies instances where the biological complexity can mask 58 measurements taken in exposure medium were obtained on an 9 simple, expected trends. Indeed, this panel does reveal which 59 Ocean Optics USB2000 spectrophotometer. For TEM studies, 5 μL of 10 bacterial strains are most critical for follow-on work and facilitates 60 a dilute solution of AuNPs was drop-cast onto a TEM grid (Ted Pella, 11 the formulation of further hypotheses. While AuNPs are the focus of 61 Redding, CA), and the AuNP sample images were taken with a JEOL 12 this work, this panel can be adapted for use with a range of 62 2100 TEM. ζ-potential measurements were obtained using a 63 Brookhaven ZetaPALS instrument.

#### **64 Bacterial Culture Conditions**

65 Bacteria were stored at -80 °C until ready for use. For S. oneidensis 66 MR-1, S. oneidensis MR-4, A. baylyi, and P. aeruginosa, the 16 Magnesium sulfate (MgSO<sub>4</sub>), sucrose, sodium molybdate dihydrate 67 appropriate bacterial stock was plated on a sterilized Luria-Bertani 4-(2-hydroxyethyl)-1-piperazineethanesulfonic 68 (LB) agar plate and incubated at 30 °C. Two colonies were inoculated 69 in 10 mL of LB broth and incubated overnight. For A. vinelandii, plates 71 two colonies were inoculated in 10 mL of Burk's medium. The 72 bacteria at late log phase were centrifuged at  $750 \times g$  for 10 min and 73 washed with Dulbecco's phosphate-buffered saline (DPBS) before 74 resuspension in HEPES buffer (2 mM HEPES, 25 mM NaCl, pH=7.4) to 75 the appropriate cell density.

#### 76 Minimum Bactericidal Concentration Determination

77 The cells were diluted in HEPES buffer to a cell density of 2×106 78 cells/mL. Cells were either exposed to PAH-AuNPs (2.81, 0.28, or 79 0.028 ppm) or to free PAH (21.16, 2.116, or 0.2116 ppm) for 10 80 minutes by mixing 180 μL of bacterial suspension with 20 μL of PAH 81 AuNP or free PAH suspension. Free PAH controls were performed 82 since the PAH AuNP suspension contained free PAH that was left over 84 in the AuNP suspensions were determined using a fluorescamine 85 assay as previously described (see ESI for fluorescamine assay 86 experimental details)35 and were used to distinguish the impact of 87 free polyelectrolyte from polyelectrolyte presented on the AuNP 88 surface. Following the 10 minute exposure, six 10 µL drops of each 89 treatment were dropped onto a dried, UV-sterilized LB agar plate 90 (Burk's medium plates were used for A. vinelandii). Once the drops 91 absorbed into the agar, the plates were incubated upside-down in a 92 30 °C incubator overnight. The PAH AuNP and free PAH 93 concentration that killed at least 99% of the bacteria were recorded.

### 95 Transmission Electron Microscopy Analysis

96 Before taking images of nanoparticle-exposed bacteria with the TEM, 97 the samples had to be embedded in epoxy resin. 7,36 At an optical 98 density of 0.8 in HEPES, the bacteria were exposed to 0.281 ppm PAH 99 AuNPs for 10 min and then washed three times in 0.1 M cacodylate <sup>49</sup> Flow Filtration Capsules, 50K MWCO, VWR). The concentrated PAH <sup>100</sup> buffer. The cells were fixed using 2.5% glutaraldehyde in 0.1 M 101 cacodylate buffer. This step proceeds for 50 min, flipping the pellet 102 after 25 min to ensure fixation. The pellet is then washed (without 103 resuspension) three times in 0.1 M cacodylate buffer.

3

4

5

6 7

8

9

10

11

12

<u>-</u>28

43

44

45

46

47 48

49

50

51

52

53

54

55

56

57

58

59 60 COMMUNICATION **Journal Name** 

To dehydrate the cells, ethanol was used at increasing 38 they exhibit different overall charges and have differing numbers of 14 using an operating voltage of 120 kV.

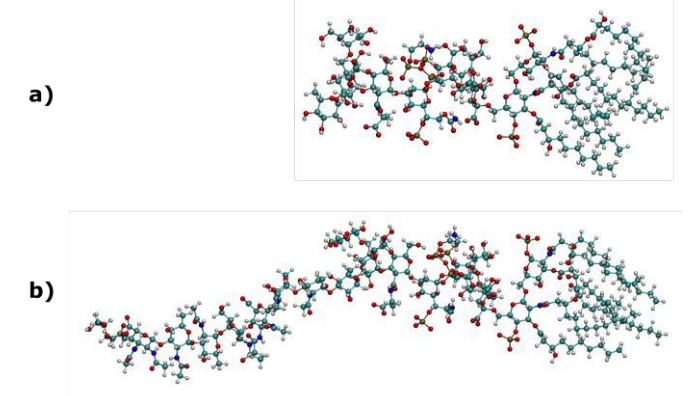


Figure 1. Ball-and-stick renderings of representative structures of a) rough LPS and b) rough LPS with two added O-antigen units onto the P. aeruginosa LPS structure.

#### 15 Flow Cytometry Analysis

16 After the bacteria reached the late log phase, they were washed in 17 DPBS and resuspended in HEPES buffer. Bacterial suspensions at 4 18 × 108 cells/mL were exposed to 2.81 ppm PAH AuNPs for 10 min and 19 then incubated with 3.34 mM SYTO9 dye at room temperature for 15 20 min. The samples were analysed with a Becton Dickenson LSRII SORP 21 flow cytometer with a 20 mW, 488 nm laser, using a control set of 22 bacteria not exposed to NPs to draw the gates. SYTO9 fluorescence 23 was used to distinguish bacteria from other debris in the sample, and 24 light scattering was used to determine which bacteria had associated 25 AuNPs. In total, each sample was done in triplicate, collecting 20,000 26 events in each run.

# 27 Computational Models and Simulation

28 The use of molecular dynamics simulations to characterize the large-29 scale association and relaxation of LPS with the PAH presented on 30 the AuNP surface can yield insight into the underlying chemistry by 31 resolving which sites, or sets of sites, induce interactions. 37,38 32 Representative model structures of the LPS molecules found on the 33 surface of P. aeruginosa, Salmonella typhimurium, and Escherichia 34 coli have been prepared. While these three structures are not perfect 35 matches for the bacteria in this panel (largely because not all the LPS 36 structures are well-known), they represent a range of LPS structures 37 and should still yield insight about critical interaction features, since

2 concentrations in water (30%, 50%, 70%, 80%, 95%, and 100% 39 phosphate units in their structure. Several Peres প্রিকার্য প্রতিষ্ঠান প্রকর্মন বিষয়ে প্রকর্মন বিষয় বিষয়ে প্রকর্মন বিষয়ে প্রমাণ বিষয়ে প্রকর্মন বিষয়ে প্রমাণ বিষয়ে প্রমাণ বিষয়ে প্রমাণ বিষয়ে প্রমাণ বিষয়ে প্রমাণ বিষয়ে প্রমাণ বিষয় বিষয় বিষয় বিষয়ে প্রমাণ বিষয়ে প্রমাণ বিষয় বিষয় বিষয় বিষয় 3 ethanol). They were rinsed three times with propylene oxide before 40 developed for prediction of interfacial properties of biological 4 being incubated with a 2:1 propylene oxide:resin mix for 2 hours 41 materials and their interactions with inorganic and organic 5 uncovered. Then they were incubated with 1:1 propylene oxide:resin 42 nanostructures. 39-42 We employed the CHARMM36 force field 6 overnight followed by 1:1 propylene oxide:resin for 4 hours and pure 43 because it is a transferable potential that has been widely used and 7 resin overnight. After replacement with fresh resin, the samples 44 benchmarked, and it presented no challenges to the numerical 8 were incubated at 40 °C for 24 hours and then 60 °C for 48 hours. The 45 convergence in the current studies. These structures have been 9 samples were cut into ~70-nm-thick sections using a LEICA EM UC6 46 energy minimized and equilibrated in the presence of 13,000 -10 ultramicrotome and stained with uranyl acetate and lead citrate to 47 25,000 explicit (TIP3P) water molecules (depending on the size of the 11 improve image contrast. The sections were placed on 200 mesh 48 system) through equations of motion driven by the CHARMM36 12 copper grids that have Formvar and carbon supports, and images 49 force field. The mixture of PAH, LPS molecules, and water is 13 were taken using a Tecnai T12 transmission electron microscope 50 neutralized through the addition of counter-ions that corresponds to 51 the number of sodium cations or chloride anions needed to 52 neutralize the "Charge of LPS + PAH" column of Table 2. For 53 simplicity, we use a 10-mer PAH construct as it provides a balance 54 between the non-chain like monomer and computationally 55 expensive long-chain polymers with hundreds or more monomeric 56 units. The chemical and molecular structure of the selected LPS have 57 been obtained from known properties of the LPS from the chosen 58 bacteria listed above. Each trajectory was then propagated for 19-20 59 nanoseconds at a cost of 65-75 hours of computer time on the XSEDE 60 Bridges regular memory nodes with 2.3 GHz Intel Xeon EP-Series 61 CPUs and 128 GB memory per CPU. In all cases, the PAH approaches 62 the LPS molecule, allowing us to consider the time to approach and 63 the location of the approach as figures of merit (or observables).

A computational study was performed to investigate PAH binding 65 using a rough LPS model and a LPS construct with "smoother" 66 character. The LPS models used here vary according to the 67 corresponding incorporation of O-antigens. The addition of two O-68 antigen units to the rough P. aeruginosa LPS was constructed using 69 the CHARM-GUI<sup>43</sup> and models a smoother construct (Fig. 1) useful for 70 our systematic study. The interaction between PAH and the LPS of Journal Name COMMUNICATION

/iew Article Online

Table 3. Minimum bactericidal concentration values observed for each bacterium after exposure to PAH AuNPs and to free PAH. The value increase after the MBC for PAH AuNPs indicates the amount of free PAH present in that concentration of PAH AuNPs as determined by the fluorescamine assay.<sup>35</sup> (Ex: 0.281 ppm of PAH AuNPs contains a free PAH concentration of 2.12 ppm). The MBCs were determined in at least triplicate measurements.

Bacteria	MBC <sub>PAH AUNPs</sub> (ppm)	Free PAH present at PAH AuNP MBC concentration (ppm)	MBC <sub>Free PAH</sub> (ppm)
A. vinelandii UW	≤0.0281	≤0.212	2.12
P. aeruginosa PAO1	≤0.0281	≤0.212	>21.2
S. oneidensis MR-4	0.281	2.12	2.12
A. baylyi ADP1	2.09	15.8	14.8
S. oneidensis MR-1	≥2.81	≥21.2	≥21.2

1*P. aeruginosa, E. coli,* and *S. typhimurium* (structures shown in Fig. 2S5), was observed through similar molecular dynamics trajectories.

The strength of the association of PAH to each LPS was evaluated 4 from trajectory simulations to better understand specific 5 interactions between the polyelectrolytes and LPS with different 6 structures. Specifically, the changes in the interaction energies 7 between the LPS and PAH are calculated after the complete 8 simulation trajectories are obtained. The effects of the water 9 molecules and ions on these energies are subtracted. Consequently, 10 the reported energies include only the contributions from the 11 interaction between the polyelectrolytes and LPS molecules.

#### 12 Results and Discussion

1 2 3

4

5

4-Publishedon 20 Occumber 2017 Downloaded by Naiversity of Wisconsin-Nadison on 1212/2012 15:15:137.

43

44

45

46

47

48

49

50 51

## 13 Synthesis and Characterization of AuNPs

14 We first verified the size of the citrate-capped AuNPs before and 15 after functionalization with PAH using several methods. Citrate-16 capped AuNPs in solution were validated after synthesis by UV-Vis 17 spectroscopy<sup>44</sup> (Fig. S2), which demonstrated that nanoparticle 18 diameter was approx. 4 nm. After functionalization with PAH, TEM 19 analysis indicated that the PAH AuNPs possessed a core diameter of  $20.4.2 \pm 1.2$  nm (n>200), and a representative TEM image is shown (Fig. 21 2). The ζ-potential of the PAH AuNPs was 46.59  $\pm$  2.63 mV. Taken 22 together, these results demonstrate that positively charged PAH 23 AuNPs were synthesized with uniform size distribution. In the 24 exposure medium, the size of the PAH AuNPs were determined to be 25 12 ± 2 nm by UV-vis extinction spectroscopy, indicating there was 26 some affiliation of the nanoparticles to each other during the  $_{27}$  exposure. The  $\zeta$ -potential of the PAH AuNPs was 34  $\pm$  2 mV, which 28 shows a slight reduction in ζ-potential in HEPES buffer, but the 29 magnitude is large enough for the particles to remain stable in 30 suspension.

#### 31 Minimum Bactericidal Concentration (MBC) Determination

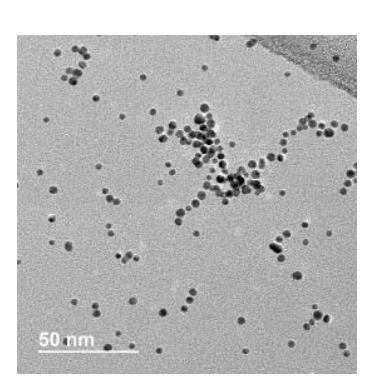


Figure 2. A representative TEM image of PAH AuNPs. Core diameter was determined to be  $4.2 \pm 1.2$  nm (n>200).

3

4

5

6 7

8

9

10

11

12

.75-18-21.0102/27/12.no.no.sides/N-coiscos/N/34/2016/18/18/18/19/2018/19/2018/19/2018/19/2018/19/2018

0% no pakinkhu42

43

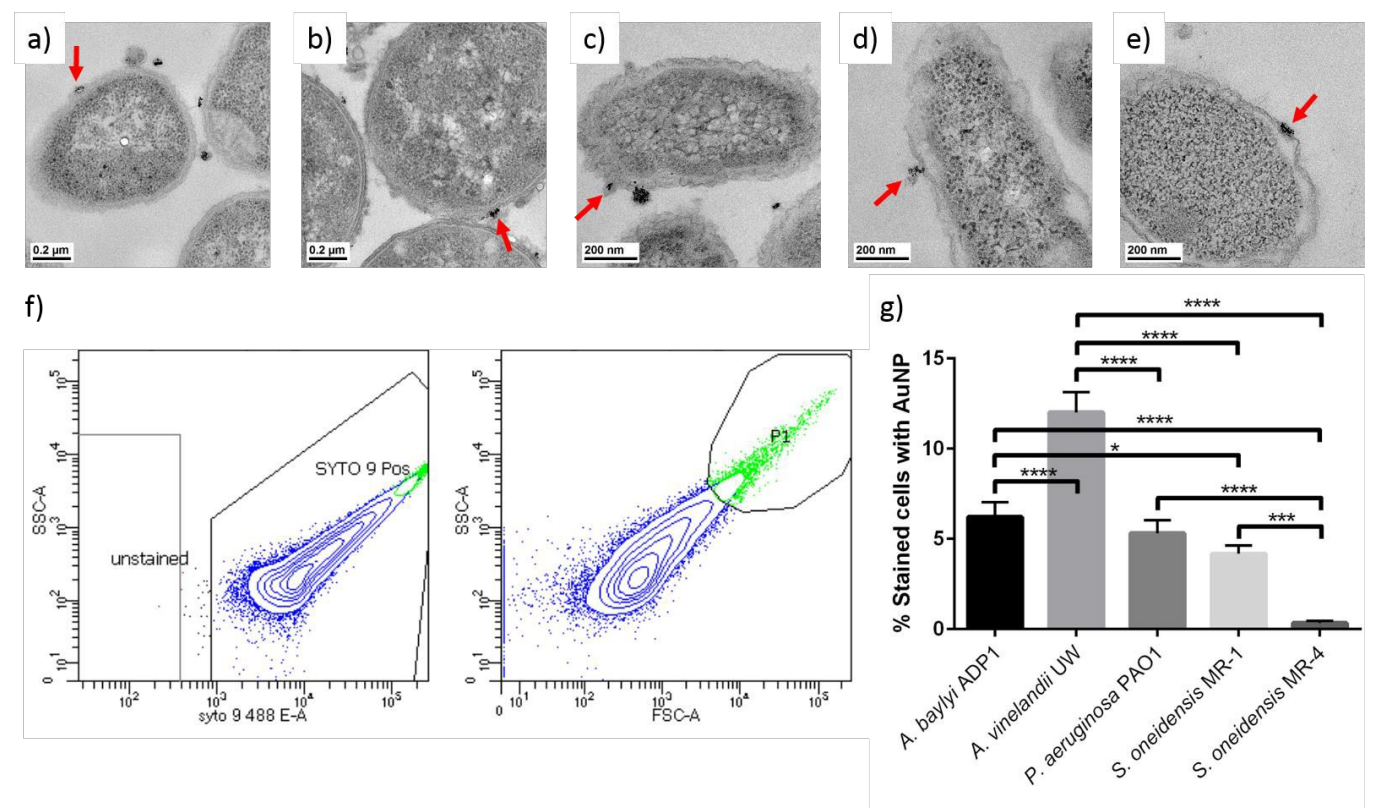
44 45

COMMUNICATION Journal Name

View Article Online DOI: 10.1039/C7EN00832E

1 To test their toxicity, the MBCs were determined for PAH AuNPs and 2 free PAH (Table 3). Each of the bacteria had different sensitivities to 3 the toxicants used in this study. The sensitivities of each bacterium 4 to PAH AuNPs are A. vinelandii = P. aeruginosa > S. oneidensis MR-4 5> A. baylyi > S. oneidensis MR-1, which was tolerant to all 6 concentrations of PAH AuNPs used in this study. The trend identified 7 by MBC shows that the toxicity cannot be as easily predicted simply 8 based on the smooth or rough character of bacterial LPS as originally 9 hypothesized, since the observed sensitivities do not follow a pattern 10 correlated with LPS type. For three of the bacteria (A. baylyi, S. 11 oneidensis MR-1, S. oneidensis MR-4), the toxicity of the PAH AuNPs 12 is explained by the free PAH that is present in those suspensions, 13 which is consistent with previous findings. 35 For A. vinelandii and P. 14 aeruginosa, a nanospecific effect is seen for the PAH AuNPs since the 15 concentration of free PAH required to kill 99% of these bacteria was 16 higher than the concentration present in the toxic PAH AuNP 17 suspensions. The wide range of sensitivities to both PAH AuNPs and 18 PAH demonstrates the importance of using a bacterial panel when 19 assessing nanoparticle properties that impact toxicity. From this 20 experiment, the two bacteria exhibiting a nanoparticle effect have 21 been identified to be used for follow-on work to study the

Figure 3. Transmission electron micrographs showing association of PAH AuNPs with a) *A. baylyi* ADP1, b) *A. vinelandii* UW, c) *P. aeruginosa* PAO1, d) *S. oneidensis* MR-1, and e) *S. oneidensis* MR-4. The red arrows show an example of PAH AuNP attachment to the bacterial cell wall. Representative flow cytometry data for f) *A. baylyi* exposed to 2.81 ppm PAH AuNPs. The left plot was used to identify cells based on the presence of SYTO9 stain, which is the boxed region of events labeled "SYTO 9 Pos". The right plot contains only the cells present in the boxed region of the left plot, and the events with both high side scattering and forward scattering were the population of cells with bound AuNPs. This gate was drawn using the maximum scattering seen in cells that were not exposed to PAH AuNPs. The blue dots correspond to cells stained with SYTO9 and the green events are stained bacterial cells that are bound to AuNPs. From flow cytometry, the percentage of cells that were bound to AuNPs are shown for the bacterial species after exposure to g) 2.81 ppm PAH AuNPs. \*p<0.05, \*\*\*p<0.001, and \*\*\*\*p<0.0001.



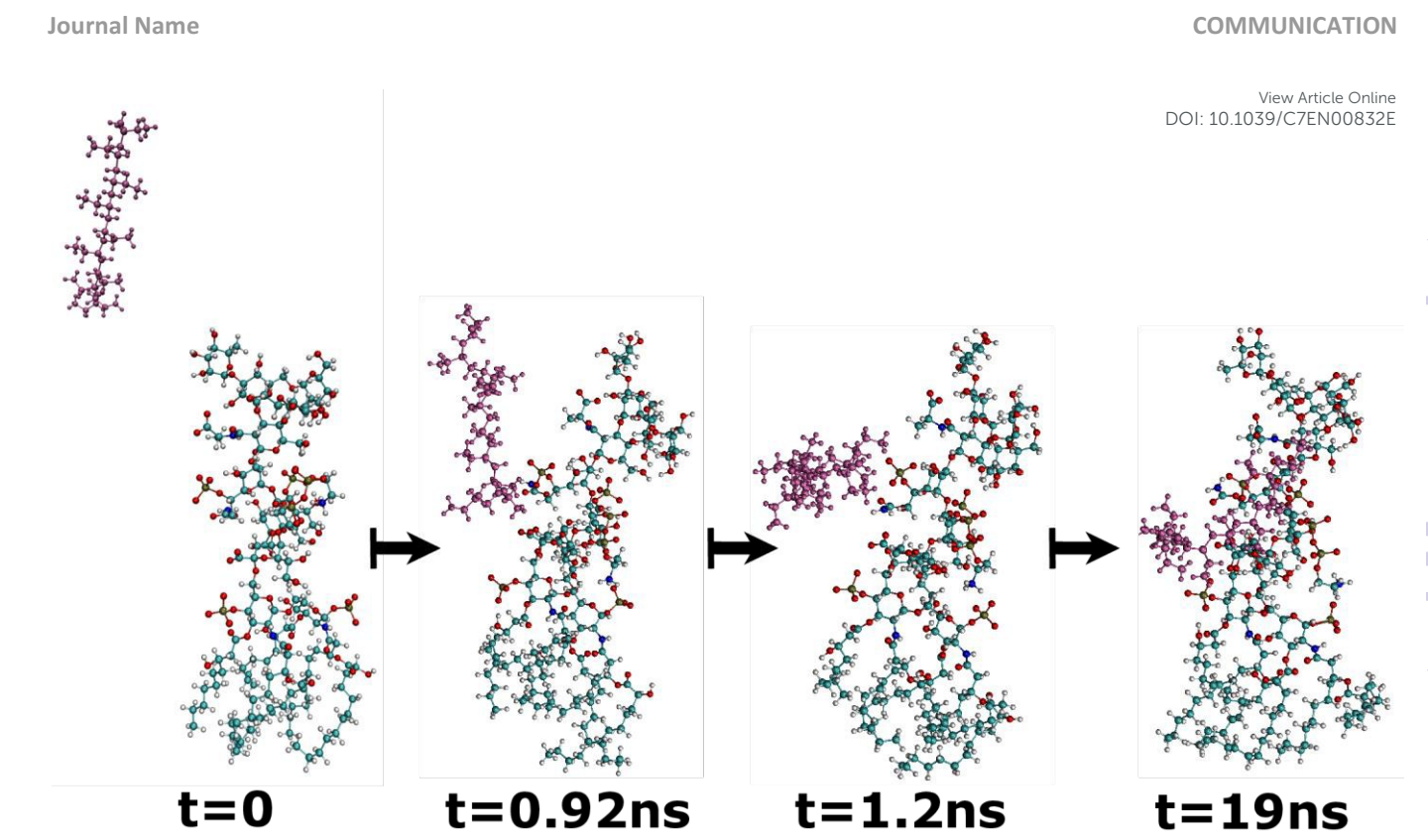


Figure 4. Snapshots of LPS from P. aeruginosa (in color-coded atoms) and PAH (with atoms in magenta) during a 19 ns simulation of the two molecules in explicit water (not shown). The PAH can be seen migrating toward the phosphate groups of the LPS.

2 three bacteria were merely experiencing the toxicity of free PAH.

### 3 Nanoparticle Association with Bacteria

1 2 3

1076 7777 7

Madisonon 1

<u>-</u>28

**⊉**9

43

44

45

46

47

48

49

50 51

52

53

54

55

56

57

58

59 60

4 Post-exposure to PAH AuNPs, the binding was visualized using TEM, 5 with examples where binding is visible shown in Fig. 3a-e. Dark field 6 TEM was utilized to confirm the presence of the diffracting AuNPs as 7 described previously (see ESI for dark field TEM images).45 The 8 images show that bound PAH AuNPs cover just a small area of the 9 bacterial cell envelope, with upwards of tens of nanoparticles bound 10 to any particular bacterium. The binding was quantified using flow 38 Computational model results 11 cytometry (Fig. 3f-g). Based on flow cytometry data, at 2.81 ppm PAH 39 While the experiments performed cannot be done at the same time-

24 interesting observations. Namely, there are instances where there 25 are similar binding amounts but different observed toxicities (i.e. P. 26 aeruginosa and S. oneidensis MR-1) and where there is similar 27 toxicity but a different amount of binding (A. vinelandii and P. 28 aeruginosa). It is often assumed that direct nanoparticle interactions

1 mechanism of toxicity for this nanoparticle type, whereas the other 29 with the cell envelope drive toxicity, and these simple relationships 30 between molecular components of the cell wall and nanoparticle 31 properties can and have been identified.7 Once you start 32 incorporating a wider range of organisms, some of these simple 33 relationships start to be masked by an increasing biological 34 complexity. This indicates that there are more complex mechanisms 35 involved in this interaction, and identifying these other mechanisms 36 will be important for each nanoparticle/bacterial interaction and can 37 lead to insight into that biological complexity.

12 AuNP, binding was seen for all bacteria except S. oneidensis MR-4, 40 scale as the computational models, simulations are used here to 13 which showed minimal binding. The order of binding from greatest 41 derive some molecular-level insight about the interaction between 14 to least is A. vinelandii (12  $\pm$  1%), A. baylyi (6.2  $\pm$  0.8%), P. aeruginosa 42 the PAH on the nanoparticle surface (modeled as a 10-mer) and LPS.  $_{15}$  (5.3  $\pm$  0.7%), S. oneidensis MR-1 (4.2  $\pm$  0.5%), and S. oneidensis MR-4  $_{43}$  Representative snapshots of the motion of PAH toward LPS (from P. 16 (0.3  $\pm$  0.1%). These data show that, in general, the bacteria with 44 aeruginosa) are shown in Fig. 4. In the first simulation, the 17 smooth LPS exhibit higher AuNP binding than those with rough LPS, 45 electrostatic association energies of PAH with rough LPS extracted 18 although for P. aeruginosa and S. oneidensis MR-1, these binding 46 from P. aeruginosa, S. typhimurium, and E. coli are monitored. The 19 amounts are very similar. We speculate that this is because the O- 47 configuration of these rough LPS are shown in Fig. S5. The number of 20 antigen of smooth LPS generally has a larger number of negatively- 48 phosphates in the core region of the LPS from S. typhimurium is one 21 charged sites for cationic nanoparticles to interact with than rough 49 unit less than that of E. coli and two units less than the P. aeruginosa 50 LPS structure, allowing consideration of the impact of the core Comparing the binding data with toxicity data reveals some 51 phosphate on association with PAH. Overall charge differences

3

4

5

6 7

8

9

10

11

12

75:15:51.21.02/21/12.no.nosiba/

<u>-</u>28

**⊉**9

₹8

ugpatished 1 42

43

44

45

46

47

48

49

50

51

52

53

54

55

56

57

58

59

60

COMMUNICATION **Journal Name** 

1 between the structures also allows for consideration of the impact of 38 structure of P. aeruginosa PAO1 has many more negatively charged 2 charge.

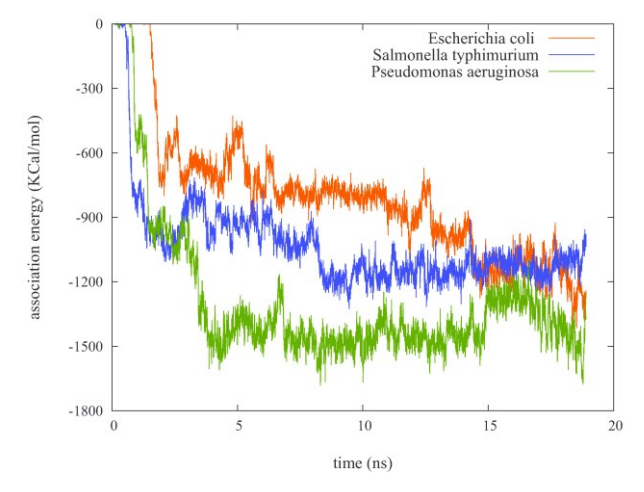


Figure 5. Electrostatic energies of the LPS/PAH association during a 19 ns simulation of 10-mer PAH interacting with the rough LPS of P. aeruginosa (green), E. coli (red), and S. typhimurium (blue) shown in Fig. S5.

The electrostatic association energies are shown in Fig. 5. The 4 PAH molecule was seen to move towards phosphate units of the core 5 region in the trajectories; the distances between the phosphorus 6 atoms and PAH through the 19 ns simulation are shown in the ESI 7 (Figs. S6-S8). These graphs suggest that the total charge of the LPS 8 and the number of the phosphate units are important parameters in 9 determining PAH association. The E. coli LPS has one unit less total 10 negative charge compared to that of S. typhimurium (Table 2). 11 Consequently, we observe a slower association of PAH to E. coli LPS. 12 However, the E. coli LPS has one phosphate unit more than the LPS 13 of S. typhimurium. The combination of these two competing factors 14 is one possible reason for the observation of nearly equal association 15 energy values at the end of the simulations for E. coli and S. 16 typhimurium LPS. On the other hand, the LPS of P. aeruginosa has a 17 higher negative charge and more phosphate units, leading to a 18 quicker association of PAH to LPS that is also stronger at the end of 19 the simulation than the other two bacteria.

We also investigated the different electrostatic association 21 energies of PAH with increasingly smooth LPS character. The degree 47 This manuscript exploits a set of bacteria which represent a 35 used here. In the case of the B-band in P. aeruginosa, for example, 36 there can be greater than 50 repeats. Future computational work will 37 build toward this more complex LPS structure. Since the B-band LPS

39 sites—because many of its sugars are amino derivatized ଫ୍ରେମ୍ପର 40 or fucose moieties, 46—this band is expected to offer more binding 41 sites for cationic particles than the more hydrophobic A-band. 42 Therefore, smooth LPS should have many more binding sites that 43 extend further into solution than those of rough LPS. This is likely why 44 we see more binding to the bacteria with smooth LPS in our 45 experimental work.

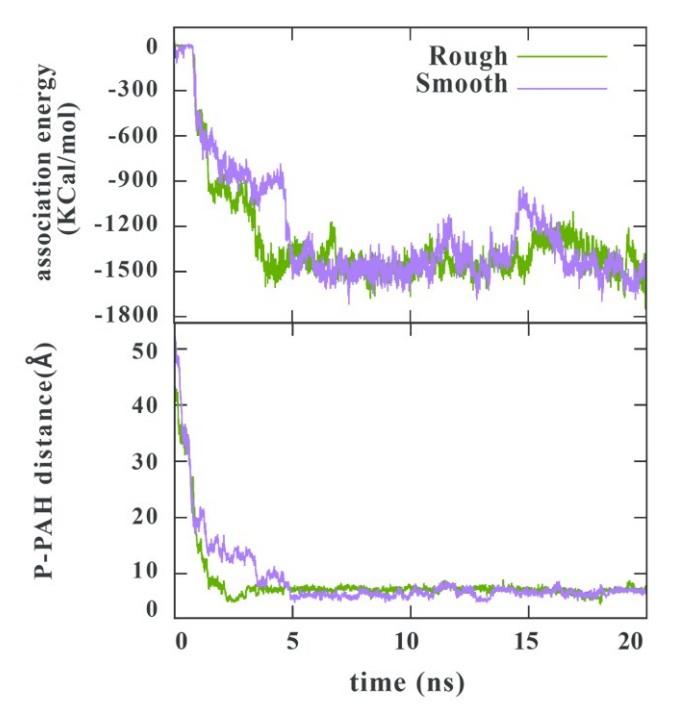


Figure 6. Electrostatic energies of the LPS/PAH association (top) and the distance between a selected phosphorus on LPS to the PAH center of mass (bottom) during a 20 ns simulation of 10-mer PAH interacting with the rough (green) and smoother (yellow) LPS constructs from P. aeruginosa shown in Fig. 2. (Note that the electrostatic energy trace for rough LPS is recapitulated from Fig. 5 to facilitate interpretation.)

#### 46 Conclusions

22 of PAH association to the rough LPS-exhibiting P. aeruginosa was 48 diverse array of environments that nanoparticles may be 23 compared to that of a smoother construct of *P. aeruginosa* with two 49 released into. These bacteria also have important ecological 24 added O-antigen units and is shown in Fig. 6. The LPS structure of P. 50 roles, making any effects felt by them impactful on overall 25 aeruginosa with two added O-antigen units has a total charge of -14. 51 environmental health. We demonstrated the use of this 26 The changes in the LPS/PAH electrostatic association energies and 52 bacterial panel in monitoring the toxicity of a model 27 the distance between a selected phosphorus atom and the PAH 53 nanoparticle, PAH AuNPs. While we observed increased PAH 28 center of mass are shown in Fig. 6. The traces in Fig. 6 suggest that 54 AuNP binding for bacteria with smooth LPS compared to those 29 PAH associates to the O-antigen sections of the smoother LPS 55 with rough LPS, the resulting toxicity did not follow this same 30 molecule at early stages of the simulation and finally moves toward 56 trend. We expected that the toxicity observed would correlate 31 the phosphate units in the core region. Moreover, the addition of 57 with the binding of these NPs to the bacteria, a process 32 two O-antigen units does not significantly slow down the overall 58 mediated by the bacterium's LPS, which is the major surface 33 movement of PAH towards the core region of LPS. Typically, smooth 59 structure, making up 75% of the Gram-negative bacterial 34 LPS has many more than the two repeats of O-antigen monomer 60 surface for some bacteria. 47 In reality, the situation is more 61 complex, which demonstrates the importance of using a 62 bacterial panel for nanotoxicity studies. Regardless of the care

Journal Name COMMUNICATION

69 11

71 12

94 18

70

 $\scriptstyle\rm 1\,in$  controlling for many variables, biology can introduce  $\scriptstyle\rm 53\,5$   $\scriptstyle\rm 2$  complexity to otherwise simple relationships.  $\scriptstyle\rm 54$ 

The increased complexity of the biological panel presented 55 6
4 here can be used for several applications. Due to the different 56
5 LPS present on the surface of these bacteria, this panel is a good 57
6 candidate for investigating bacterial surfaces. Indeed, the 58
7 results obtained from the molecular dynamics simulation yield 59 7
8 early insight into the interactions of polyelectrolyte-wrapped 60
9 NPs with bacteria by taking the sugar sequences of the LPS into 61
10 account. This panel is also good for an initial screen of 62
11 nanoparticle toxicity; in using this bacterial panel, we can 63 8
12 identify which bacteria are experiencing an effect specific to 64
13 nanoparticles, which merit further investigation. While we 65 9
14 would expect different results than those presented here if 66
15 different NPs were used, this Gram-negative bacterial panel can 67 10
16 be adapted for use with a range of nanomaterials.

# 17 Acknowledgements

1

3

4

5

6

7

8

9

10

11

12

7515-51-71 73 4 5-1-71 5-1-71 5-1-71 5-1-71

Madison on 21/12/2010

<u>-</u>28

**⊉**9

December 2017, Downhaded

₹8

43

44

45

46

47

48

49

50

51

52

53

54

55

56

57

58

59 60

18 This work was supported by the National Science Foundation 72 19 under the Center for Sustainable Nanotechnology, CHE- 73 20 1503408. J.T.B. was supported by the University of Minnesota 74 13 21 Biotechnology Training Grant Program through the National 75  $_{
m 22}$  Institutes of Health. K.M.L. was supported by a University of  $^{76}$   $^{14}$  $^{23}$  Minnesota UROP award. We are grateful to Tian (Autumn) Qiu  $^{77}$ 24 for her work with the fluorescamine assay. The authors 78 15 25 gratefully acknowledge Dr. Michael P. Schwartz, Dr. Joel A. 79  $_{26}$  Pedersen, and Dr. Franz M. Geiger for helpful discussion. The  $^{80}\,16$ 27 TEM work in this study was carried out in the Characterization 81 28 Facility, University of Minnesota, which receives partial support 82  $_{\rm 29}$  from NSF through the MRSEC program. We thank Fang Zhou for  $\,^{\rm 83}$  $_{
m 30}$  microtome sectioning of the resin-embedded bacteria samples  $^{
m 84}$   $^{
m 17}$ 31 for TEM analysis. The authors are grateful for the University of 85 32 Minnesota's University Flow Cytometry Resource for flow 86 33 cytometric analysis.

The computing resources necessary for this research were 88 provided in part by the National Science Foundation through 89 provided in part by the National Science Foundation through 89 provided in part by the National Science Foundation through 89 provided National Computing Center (Marcol.) 92 provided by 91 provided by 91 provided Maryland Advanced Research Computing Center (Marcol.) 92 provided by 91 provided Maryland Advanced Research Computing Center (Marcol.) 92 provided by 91 provided Maryland Advanced Research Computing Center (Marcol.)

#### 39 References

40 1	C. J. Murphy, A. M. Vartanian, F. M. Geiger, R. J. Hamers, J.	96
41	Pedersen, Q. Cui, C. L. Haynes, E. E. Carlson, R. Hernandez,	97
42	R. D. Klaper, G. Orr and Z. Rosenzweig, ACS Cent. Sci., 2015,	98
43	<b>1</b> , 117–123.	99
44 2	R. Eigenheer, E. R. Castellanos, M. Y. Nakamoto, K. T.	100
45		101
46	2014, <b>1</b> , 238–247.	102 19
47 3	S. Naeem, D. R. Hahn and G. Schuurman, <i>Nature</i> , 2000,	103
48	<b>403</b> . 762–764.	104 20
49 <b>4</b>	J. Borcherding, J. Baltrusaitis, H. Chen, L. Stebounova, CM.	105
50	Wu, G. Rubasinghege, I. A. Mudunkotuwa, J. C. Caraballo, J.	106 21
51		107
52	Nano, 2014, <b>1</b> , 123–132.	108 22
J.		109

A.-K. Ostermeyer, C. K. Mumuper, L. Semprini, and Ticle Online Radniecki, *Environ. Sci. Technol.*, 2019, 47, 1740321441652E I. L. Gunsolus, M. N. Hang, N. V Hudson-Smith, J. T. Buchman, J. W. Bennett, D. Conroy, S. E. Mason, R. J. Hamers and C. L. Haynes, *Environ. Sci. Nano*, 2017, **4**, 636–646.

Z. V. Feng, I. L. Gunsolus, T. A. Qiu, K. R. Hurley, L. H. Nyberg, H. Frew, K. P. Johnson, A. M. Vartanian, L. M. Jacob, S. E. Lohse, M. D. Torelli, R. J. Hamers, C. J. Murphy and C. L. Haynes, *Chem. Sci.*, 2015, **6**, 5186–5196. L. Liu, J. Yang, J. Xie, Z. Luo, J. Jiang, Y. Y. Yang and S. Liu, *Nanoscale*, 2013, **5**, 3834–3840.

Z. Li, K. Greden, P. J. J. Alvarez, K. B. Gregory and G. V
Lowry, *Environ. Sci. Technol.*, 2010, 44, 3462–3467.
Y. Zhao, Z. Chen, Y. Chen, J. Xu, J. Li and X. Jiang, *J. Am. Chem. Soc.*, 2013, 135, 12940–12943.

C. M. Goodman, C. D. McCusker, T. Yilmaz and V. M. Rotello, *Bioconjug. Chem.*, 2004, **15**, 897–900. Y. Tu, M. Lv, P. Xiu, T. Huynh, M. Zhang, M. Castelli, L. Zengrong, Q. Huang, C. Fan, H. Fang and R. Zhou, *Nat. Nanotechnol.*, 2013, **8**, 594–601.

R. Y. Pelgrift and A. J. Friedman, *Adv. Drug Deliv. Rev.*, 2013, **65**, 1803–1815.

O. Bondarenko, A. Ivask, A. Käkinen, I. Kurvet and A. Kahru, *PLoS One*, 2013, **8**, e64060.

H. A. Foster, I. B. Ditta and S. Varghese, *Appl. Microbiol. Biotechnol.*, 2011, **90**, 1847–1868.

K. H. Jacobson, I. L. Gunsolus, T. R. Kuech, J. M. Troiano, E. S. Melby, S. E. Lohse, D. Hu, W. B. Chrisler, C. J. Murphy, G. Orr, F. M. Geiger, C. L. Haynes and J. A. Pedersen, *Environ. Sci. Technol.*, 2015, **49**, 10642–10650.

J. C. Setubal, P. dos Santos, B. S. Goldman, H. Ertesvåg, G. Espin, L. M. Rubio, S. Valla, N. F. Almeida, D. Balasubramanian, L. Cromes, L. Curatti, Z. Du, E. Godsy, B. Goodner, K. Hellner-Burris, J. A. Hernandez, K. Houmiel, J. Imperial, C. Kennedy, T. J. Larson, P. Latreille, L. S. Ligon, J. Lu, M. Maerk, N. M. Miller, S. Norton, I. P. O'Carroll, I. Paulsen, E. C. Raulfs, R. Roemer, J. Rosser, D. Segura, S. Slater, S. L. Stricklin, D. J. Studholme, J. Sun, C. J. Viana, E. Wallin, B. Wang, C. Wheeler, H. Zhu, D. R. Dean, R. Dixon and D. Wood, J. Bacteriol., 2009, 191, 4534-4545. L. Dijkshoorn, A. Nemec, M. Vaneechoutte, T. De Baere, R. A. Pantophlet, P. A. Williams, C. M. Kay, B. Averhoff, I. Graf, L. N. Ornston, S. Schlimpert, A. Buchan, D. Parke, S. H. Craven, O. C. Ezezika, C. Momany, E. L. Neidle, U. Gerischer, B. Jerg, R. Fischer, D. L. Gutnick, H. Bach, A. P. Tomaras, C. W. Dorsey, C. McQueary, L. A. Actis, H. Seifert,

Academic Press, Norfolk, UK, 2008. V. de Berardinis, M. Durot, J. Weissenbach and M. Salanoubat, *Curr. Opin. Microbiol.*, 2009, **12**, 568–576. H. H. Hau and J. A. Gralnick, *Annu. Rev. Microbiol.*, 2007, **61**, 237–258.

H. Wisplinghoff and K. J. Towner, ed. U. Gerischer, Caister

E. Vinogradov, J. Kubler-Kielb and A. Korenevsky, *Carbohydr. Res.*, 2008, **343**, 2701–2705.

J. B. Morrow, C. Arango Pinedo and R. D. Holbrook, *J. Environ. Qual.*, 2010, **39**, 1934–1941.

59

61 62 **49** 

64

66 67

68

69

70

72

74 75

73 51

65 50

60 48

1

3

4

5

6

7

8

9

10

11

12

	IMUNICATION
1 23	G. B. Pier, Int. J. Med. Microbiol., 2007, <b>297</b> , 277–295.
2 24	H. L. Rocchetta, L. L. Burrows and J. S. Lam, <i>Microbiol. Mol.</i>
3	Biol. Rev., 1999, <b>63</b> , 523–553.
4 25	E. Vinogradov, A. Korenevsky and T. J. Beveridge,
5	Carbohydr. Res., 2003, <b>338</b> , 1991–1997.
6 <b>26</b>	P. Zhao, N. Li and D. Astruc, Coord. Chem. Rev., 2013, 257,
7	638–665.
8 2 7	D. A. Giljohann, D. S. Seferos, W. L. Daniel, M. D. Massich,
9	P. C. Patel and C. A. Mirkin, <i>Angew. Chemie Int. Ed. Engl.</i> , 2010, <b>49</b> , 3280–3294.
10 11 <b>28</b>	A. Gole and C. J. Murphy, <i>Chem. Mater.</i> , 2005, <b>17</b> , 1325–
12	1330.
13 29	J. J. Richardson, J. Cui, M. Björnmalm, J. A. Braunger, H.
14	Ejima and F. Caruso, <i>Chem. Rev.</i> , 2016, <b>116</b> , 14828–14867.
15 30	P. Gentile, I. Carmagnola, T. Nardo and V. Chiono,
16	Nanotechnology, 2015, <b>26</b> , 422001.
17 31	Y. Zhou, Y. Kong, S. Kundu, J. D. Cirillo and H. Liang, J.
18	Nanobiotechnology, 2012, <b>10</b> , 19.
19 32	T. A. Qiu, J. S. Bozich, S. E. Lohse, A. M. Vartanian, L. M.
20	Jacob, B. M. Meyer, I. L. Gunsolus, N. J. Niemuth, C. J.
21	Murphy, C. L. Haynes and R. D. Klaper, Environ. Sci. Nano,
22	2015, <b>2</b> , 615–629.
23 33	A. Gole and C. J. Murphy, <i>Chem. Mater.</i> , 2004, <b>16</b> , 3633–
24	3640.
25 34	J. W. Newton, P. W. Wilson and R. H. Burris, J. Biol. Chem.,
26 27 <b>2</b> E	1953, <b>204</b> , 445–451.
27 <b>35</b> 28	T. A. Qiu, M. D. Torelli, A. M. Vartanian, N. B. Rackstraw, J. T. Buchman, L. M. Jacob, C. J. Murphy, R. J. Hamers and C.
29	L. Haynes, <i>Anal. Chem.</i> , 2017, <b>89</b> , 1823–1830.
30 <b>36</b>	A. M. Schrand, J. J. Schlager, L. Dai and S. M. Hussain, <i>Nat.</i>
31	<i>Protoc.</i> , 2010, <b>5</b> , 744–757.
32 <b>37</b>	Q. Cui, R. Hernandez, S. E. Mason, T. Frauenheim, J. A.
33	Pedersen and F. Geiger, J. Phys. Chem. B, 2016, 120, 7297-
34	7306.
35 <b>38</b>	E. L. Wu, O. Engström, S. Jo, D. Stuhlsatz, M. S. Yeom, J. B.
36	Klauda, G. Widmalm and W. Im, Biophys. J., 2013, 105,
37	1444–1455.
38 39	Z. Cournia, J. C. Smith and G. M. Ullmann, J. Comput.
39	Chem., 2005, <b>26</b> , 1383–1399.
40 40	F. S. Emami, V. Puddu, R. J. Berry, V. Varshney, S. V
41	Patwardhan, C. C. Perry and H. Heinz, <i>Chem. Mater.</i> , 2014,
42 43 <b>41</b>	<b>26</b> , 2647–2658. H. Heinz, TJ. Lin, R. K. Mishra and F. S. Emami, <i>Langmuir</i> ,
43 <b>4 1</b> 44	2013, <b>29</b> , 1754–1765.
45 <b>42</b>	TJ. Lin and H. Heinz, <i>J. Phys. Chem. C</i> , 2016, <b>120</b> , 4975–
46	4992.
47 43	S. Jo, X. Cheng, J. Lee, S. Kim, SJ. Park, D. S. Patel, A. H.
48	Beaven, K. II Lee, H. Rui, S. Park, H. S. Lee, B. Roux, A. D.
49	Mackerell Jr, J. B. Klauda, Y. Qi and W. Im, J. Comput.
50	Chem., 2017, <b>38</b> , 1114–1124.
51 44	W. Haiss, N. T. K. Thanh, J. Aveyard and D. G. Fernig, Anal.
52	Chem., 2007, <b>79</b> , 4215–4221.
53 <b>45</b>	N. D. Klein, K. R. Hurley, Z. V. Feng and C. L. Haynes, <i>Anal.</i>
54	Chem., 2015, <b>87</b> , 4356–4362.
55 <b>46</b>	J. S. Lam, L. L. Graham, J. Lightfoot, T. Dasgupta and T. J.
56	Beveridge, <i>J. Bacteriol.</i> , 1992, <b>174</b> , 7159–7167.

A. P. Le Brun, L. A. Clifton, C. E. Halbert, B. Lin, M. Meron,

DOI: 10.1039/C7EN00832E 2013, **14**, 2014–2022. H. Rediers, J. Vanderleyden and R. De Mot, Microbiology, 2004, **150**, 1117–1119. G. Gaona, C. Nuñez, J. B. Goldberg, A. S. Linford, R. Nájera, M. Castañeda, J. Guzmán, G. Espín and G. Soberón-Chávez, FEMS Microbiol. Lett., 2004, 238, 199-206. C. K. Stover, X. Q. Pham, A. L. Erwin, S. D. Mizoguchi, P. Warrener, M. J. Hickey, F. S. L. Brinkman, W. O. Hufnagle, D. J. Kowalik, M. Lagrou, R. L. Garber, L. Goltry, E. Tolentino, S. Westbrock-Wadman, Y. Yuan, L. L. Brody, S. N. Coulter, K. R. Folger, A. Kas, K. Larbig, R. Lim, K. Smith, D. Spencer, G. K.-S. Wong, Z. Wu, I. T. Paulsen, J. Reizer, M. H. Saier, R. E. W. Hancock, S. Lory and M. V Olson, Nature, 2000, 406, 959-964. C. S. Hong, M. Shitashiro, A. Kuroda, T. Ikeda, N. Takiguchi, H. Ohtake and J. Kato, FEMS Microbiol. Lett., 2004, 231,

P. J. Holden, J. H. Lakey and S. A. Holt, Biomacromolecules, and S. A. Holt, Biomacrom

**Journal Name** 

57 **47** 

59

60

